AIAA 84-1430

Design of Long-Endurance Unmanned Airplanes Incorporating Solar and Fuel Cell Propulsion

J. W. Youngblood, T. A. Talay, and R. J. Pegg
NASA Langley Research Center, Hampton, Virginia

AIAA/SAE/ASME
20th Joint Propulsion Conference
June 11-13, 1984
Cincinnati, Ohio

DESIGN OF LONG-ENDURANCE UNMANNED AIRPLANES INCORPORATING SOLAR AND FUEL CELL PROPULSION

James W. Youngblood*
Theodore A. Talay*
and
Robert J. Pegg**
NASA Langley Research Center
Hampton, Virginia 23665

Abstract

Preliminary performance analysis and conceptual design are described for a class of unmanned airplanes possessing multi-day endurance capability. A mixed-mode electric power system incorporates solar cells for daytime energy production and a non-regenerative H_2-O_2 fuel cell to supply energy for night flight. The power system provides energy for all onboard systems, including propulsion, payload, and avionics. Excess solar energy is available during significant portions of the day, and may be used for climbing, maneuvering, or payload functions. By jettisoning fuel cell reactant product (water) during flight, vehicle endurance may be increased under certain conditions. Empirical structure sizing algorithms are combined with low-Reynolds number aerodynamics algorithms to estimate airplane size and geometry to meet prescribed mission requirements.

Initial calculations for summertime, high-altitude flight (above 40,000 ft (12 km)) at moderate latitude (31° N) indicate that mission endurance of several days may be possible for configurations having wing loadings on the order of 0.9 to 1.3 lb/ft^2. These aircraft tend to be somewhat smaller than solar-powered aircraft previously conceived for multi-month endurance utilizing regenerative fuel cell systems for night flight.

Introduction

Since the manned, solar-powered, Paris-to-London flight of Dr. Paul MacCready's Solar Challenger airplane in 1981,[1] efforts have continued to develop technology for an unmanned solar-powered aircraft which can cruise for extended periods (weeks) at high altitudes (above 40,000 ft (12 km)). Potential uses for such a remotely piloted airborne platform have been discussed in the literature.[2-3] Previous studies have assumed that the on-board energy storage medium (secondary battery or regenerative fuel cell) will be recharged by solar energy for nighttime cruise. Although flight endurance of weeks or months is theoretically attainable in this mode, the requirement for concurrent collection of sufficient solar energy for recharging and direct propulsion gives rise to very large airplanes. The feasibility of such airplanes is open to question because of simultaneous burdens placed on several key, enabling technologies: strong, lightweight materials for airframe structure; low Reynolds number aerodynamics for design of propellers and lifting surfaces; and high efficiency, lightweight power train components (electric motors and controllers, solar cells, and fuel cells).

To relax, somewhat, these subsystem technology requirements (at the expense of cruise endurance and altitude) and approach a current "state of the art," we consider here an adaptation of the hydrogen-oxygen fuel cell currently installed and flying on the Space Transportation System's Orbiter vehicle. In our scenario, solar energy satisfies all onboard energy requirements during daylight hours. The fuel cell, which is non-regenerative, meets all energy requirements, including propulsion, payload, and avionics, through successive night cycles until the reactants (H_2 and O_2) are depleted, at which time the airplane glides down for recovery and recycling. Since the fuel cell will produce power for night flight so long as reactants inflow is uninterrupted, the major modification to existing fuel cell hardware is to tailor reactant tankage volume to meet endurance objectives.

This paper presents a brief description of our airplane concept and some preliminary performance and sizing results. These results are based on empirical relationships derived for the purpose of bounding this particular problem.

Symbols

A, B	constants in equation (1)
AR	wing aspect ratio
b	wing span, ft
C_D	drag coefficient
C_{D_o}	drag coefficient at zero lift
C_L	lift coefficient
$C_{L_{wind}}$	maximum, wind-limited value of lift coefficient
e	airplace efficiency factor
H	altitude, ft (km)
N	number of night cycles
n	ultimate structural load factor

*Aero-Space Technologist, Space Systems Division; Member, AIAA
**Aero-Space Technologist, Systems Engineering Division

P	power, watts
S	area, ft^2
T	period of night operation, hours
V	velocity, ft/sec.
V_{wind}	wind velocity, ft/sec.
W	weight, lbs
π	3.14159
ρ	atmospheric density, $slugs/ft^3$ (1976 U.S. Standard Atmosphere)

Subscripts

af	airframe
av	avionics
b	booms
fc	fuel cell
ht	horizontal tail
max	maximum
p	pod
pay	payload
prop	propulsion drive system
r	reactants
rad	radiator
sc	solar cells
t	tail
ta	tankage
tot	total
vt	vertical tail
w	wing

Baseline Mission

A hypothetical mission, proposed by the Water Conservation Laboratory, U.S. Department of Agriculture, requires remote radiometric observations of summertime agricultural phenomena in south central Arizona. The mission would take place within 30 days of the summer solstice (June 21) to ensure high insolation and to take advantage of seasonally low wind speeds prevailing at a nominal cruise altitude of 49200 ft (15 km). The payload is assumed to weigh 100 pounds and draw 300 watts of power.

Description of Airplane

The all-electric airplane configuration is akin to that described in earlier work[2] and is illustrated in Fig. 1. It may be characterized as an unmanned, remotely controlled, twin-propeller monoplane with twin-boom empennage supporting a large horizontal stabilizer and twin rudders. A central pod housing payload, propulsion, avionics, and other systems is mounted under the wing. The avionics package weighs 140 pounds and draws 500 watts of power. Photovoltaic solar cells are installed on upper surfaces of the wing and horizontal stabilizer.

Several other assumptions are inherent in our analysis. First, the airplane is in level, unaccelerated flight. Calculations of available solar energy assume that solar arrays are horizontal. (Additional solar cells can be mounted on vertical rudder surfaces, although we have not accounted for this additional system mass or energy input in present calculations.) All onboard systems are powered by direct insolation during the day and by the fuel cell at night. Launch and recovery are not treated; however, it is assumed that, weather permitting, the vehicle can climb to its operational altitude under direct insolation after an early morning launch. Finally, the reactant waste product (water) may be dumped overboard to reduce gross weight during flight, thereby improving airplane endurance to some degree.

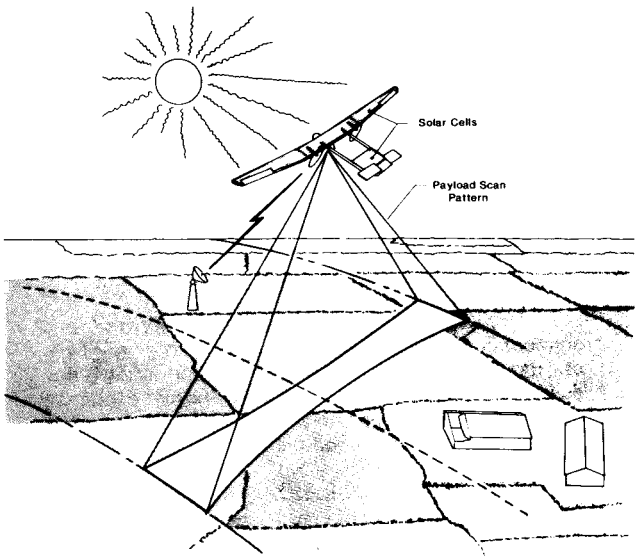

Fig. 1 Representative airplane configuration in cruise flight.

Power System

Figure 2 is a diagram of the proposed power system. The system includes the H_2-O_2 fuel cell primary energy storage system for nighttime use and solar cell arrays for daytime power. Power is transmitted to each propeller by a separate electric motor.

Solar Cells - Spectral response of a representative solar cell[4] is shown in Fig. 3. For particular date, latitude, and altitude, this wave-length dependent response characteristic can be combined with calculated intra-atmosphere solar radiant flux densities to compute the power available from the cell as a function of time. The solar cell power output curve shown in Fig. 4 is for the chosen mission conditions (July 21, 31° N latitude) and was calculated for 39,400 ft (12 km) altitude, which produces slightly conservative performance results for higher altitudes. Superimposed on Fig. 4 is the curve illustrating power required to maintain straight and level cruise flight. Fuel cell power is phased in and out at sunset and sunrise, respectively. For the mission date chosen, design power level per unit collector area is $P_{tot}/S_{sc}=5.5$ w/ft^2. The

effective night interval of fuel cell operation is T=12.5 hours. It is important to minimize P_{tot}/S_{sc} and T to minimize fuel cell reactant loading, as will be shown later. Note that during daylight hours, a substantial amount of "excess" solar energy will be available for climbing, maneuvering, or payload augmentation.

Fuel Cells - The H_2-O_2 fuel cell system characteristics used in this study are based on the state of the art unit installed in the Space Shuttle Orbiter. The fuel cell assembly includes a reactor vessel (power section) and an accessory section (for control of reactant flow and power output). Individual cells may be combined (stacked) in the power section to produce a desired output voltage. For purposes of this study, average single-cell voltage is 0.9 volt, and average current density is 200 amps per ft^2. Because high motor efficiencies can be obtained at high voltages, an operating voltage of 105 Vdc is selected for the maximum overall power section output. To accommodate the range of performance parameters developed in this study, it is assumed that the fuel cell can be throttled between 2 and 12 kw, its maximum continuous power output level. Weight of the fuel cell system is 300 pounds, including the accessory section weighing 65 pounds and the power section weighing 235 pounds. Overall dimensions are approximately 4 ft. long x 1.25 ft. wide x 1.25 ft. high. Reactant consumption (and water production) is approximately 0.835 pound per kw-hr. Waste heat from the exothermic operation of the cell is approximately 2,100 BTU/kw-hr, and is handled by flat-plate radiators located in the wing or in the pod. High-pressure tanks for the reactant gases are assumed to be made of high strength, filament wound Kevlar 49, with thin metal liners.

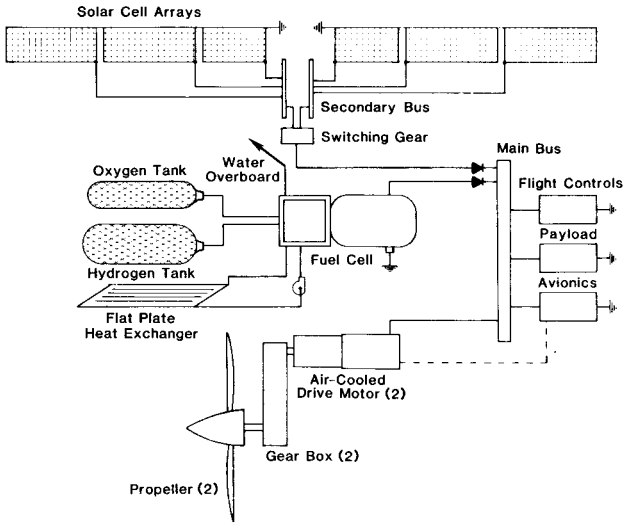

Fig. 2 Diagram of airplane power system.

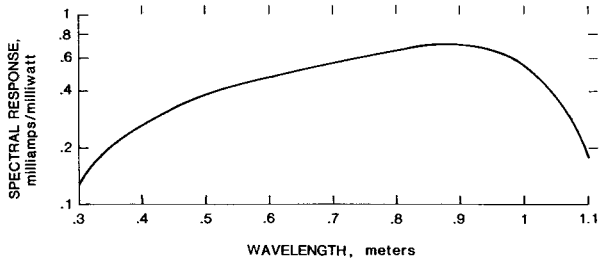

Fig. 3 Spectral response of representative silicon solar cell (Ref. 4).

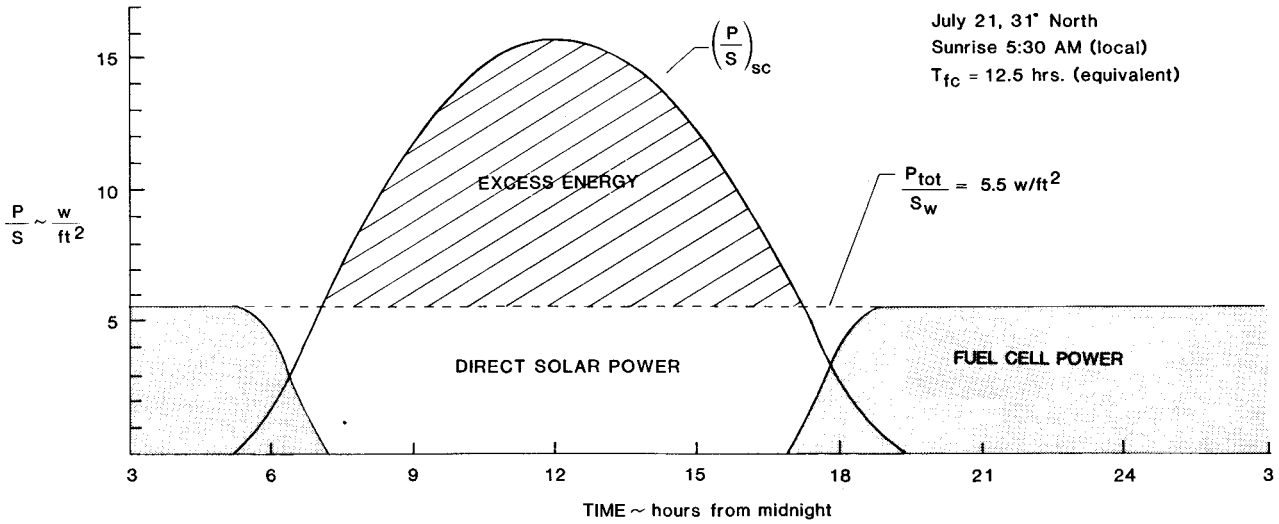

Fig. 4 Profiles of solar power available and total power required.

Drive Train - The vehicle concept employs two pusher-type propellers, each driven by an air-cooled electric motor. Each motor drive system has its own electric controller and inverter. Additionally, there is an avionics interface between the two systems to balance thrust. High-speed, rare-Earth, permanent magnet brushless motors[5] are used, each incorporating appropriate speed reduction systems to drive large, relatively slow-turning propellers.

Airplane Structures and Sizing Algorithm

The airplane consists of airframe, propulsion drive system, solar cell, fuel cell, avionics, and payload subsystems. Airframe weights are estimated parametrically using an expression derived in Ref. 6 for sailplanes

$$W_{af} = A\left(nS_w b^3\right)^B \tag{1}$$

Data and calculated estimates of airframe weight, ultimate loads, and airplane geometry of MacCready's Solar Challenger and a recent large, high-altitude solar-powered airplane design concept[7] were used in a regression analysis to define A = 0.310 and B = 0.311 for a class of ultralight, cantilever wing airplanes with twin boom tails. Using the aspect ratio relation

$$AR = \frac{b^2}{S_w} \tag{2}$$

equation (1) can be rewritten as an airframe weight loading

$$\frac{W_{af}}{S_w} = .31n^{.311} S_w^{-.222} AR^{.467} \tag{3}$$

Propulsion drive system weight W_{prop} is scaled linearly with thrust power based on the motor and propeller design from the Solar Challenger and the samarium-cobalt motor-controller system described in Ref. 5. As a weight loading, it is expressed as

$$\frac{W_{prop}}{S_w} = .0114 \frac{P_{prop}}{S_w} \tag{4}$$

The solar cell arrays (and associated wiring) weight loading is estimated as

$$\frac{W_{sc}}{S_w} = .15 \tag{5}$$

which is in the range of previous solar-powered airplanes.[8,9] This weight loading takes into account that the combined effective cell area on the wing and horizontal stabilizer is 82 percent of the wing planform area.

The fuel-cell system weight loading is given as

$$\frac{W_{fc}}{S_w} = \frac{300}{S_w} \tag{6}$$

The fuel-cell reactant and associated tankage weights depend on the total power level (P_{tot}) required for propulsion (P_{prop}), payload (P_{pl}) and avionics (P_{av}), and the required period of night operation (NT). Weight loading of the reactants is given by

$$\frac{W_r}{S_w} = .000835\ (NT) \frac{P_{tot}}{S_w} \tag{7}$$

From data contained in Ref. 10, reactant tankage weight loading is estimated by

$$\frac{W_{ta}}{S_w} = .000658\ (NT) \frac{P_{tot}}{S_w} \tag{8}$$

and radiator system weight loading is estimated by

$$\frac{W_{rad}}{S_w} = .0015\left(\frac{P_{tot}}{S_w}\right) + \frac{30}{S_w} \tag{9}$$

The avionics and payload packages are fixed at 140 pounds and 100 pounds, respectively. As weight loadings, these are

$$\frac{W_{av}}{S_w} = \frac{140}{S_w} \tag{10}$$

and

$$\frac{W_{pay}}{S_w} = \frac{100}{S_w} \tag{11}$$

Given a total wing loading for the airplane W_{tot}/S_w, the computational procedure is to subtract the component weight loadings given in equations (3)-(11) to determine the allowable weight loading for the airframe.

$$\frac{W_{af}}{S_w} = \frac{1}{S_w}\left(W_{tot} - W_{prop} - W_{sc} - W_{fc} - W_r - W_{ta} - W_{rad} - W_{av} - W_{pay}\right) \tag{12}$$

Equation (3) can be rearranged to give an expression for airplane wing aspect ratio AR in terms of the allowable airframe weight loading, wing area, and ultimate load factor n

$$AR = \left(\frac{W_{af}}{S_w} \cdot \frac{S_w^{.222}}{.31n^{.311}}\right)^{2.142} \tag{13}$$

Equations (12) and (13) can be combined to yield a detailed description of airplane size and subsystem weight allocations. Although an earlier study of large, solar-powered airplanes[11] was based on a design load factor of 2, we have chosen a load factor of 4 to account for structural loading anticipated during launch and recovery operations.

For a chosen total wing loading, therefore, sufficient information is available in equations (3) through (13) to describe the airplane in terms of individual subsystem weights, aspect ratio, and wingspan as a function of wing area alone. This provides the input necessary for the aerodynamics algorithms shown in Fig. 5.

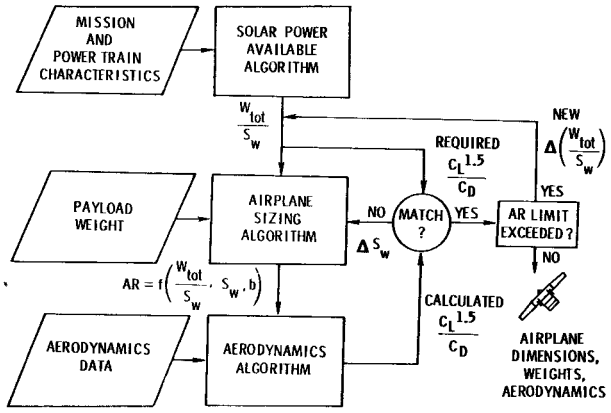

Fig. 5 Airplane design procedure.

Aerodynamics Algorithms

To satisfy the aerodynamic requirements of the cruise condition, the endurance parameter $C_L^{1.5}/C_D$ based on an estimate of vehicle aerodynamics must equal or exceed the value dictated by thrust power available. The following assumptions are made to estimate the airplane aerodynamics.

The Wortmann FX 63-137 airfoil section is chosen for the wing in the anticipated Reynolds number range of 10^5 to 10^6. This airfoil section has been used previously for low-speed, man-powered airplanes.[12] Lift and drag coefficient data for the section are obtained from Ref. 13. The wing consists of three equal span panels, with the outer-panel chord length tapering to half the root chord length. The zero-lift wing-profile drag coefficient C_{D_o} is a composite average of the root and tip section coefficients at the appropriate Reynolds number, based on data in Ref. 13.

Horizontal and vertical tail surfaces generally operate at low values of C_L; therefore, their lift-dependent drag contributions to overall drag are considered to be small. Utilizing a thin, low-drag airfoil section (NACA 0008-34) an estimate of zero-lift tail drag coefficient, based on Ref. 14, is

$$\left(C_{D_o}\right)_t = \frac{.0065}{S_w}\left(S_{ht} + S_{vt}\right) \qquad (14)$$

where S_{ht} and S_{vt} are horizontal and vertical tail areas, respectively. The horizontal tail is oversized to provide additional solar cell mounting area (S_{ht}/S_w=0.31). The twin vertical tail surfaces together are sized by S_{vt}/S_w=0.10.

A low-drag pod is centrally mounted on a pylon beneath the wing. The pod and pylon house the fuel cell, reactant tanks, avionics, radiator, and payload systems. At a Reynolds number of 1 x 10^6, Ref. 15 shows a drag coefficient of 0.06 based on pod cross-sectional area for a 3:1 length:diameter ratio. Referencing drag coefficient to the wing area gives

$$\left(C_{D_o}\right)_p = .0007 \qquad (15)$$

Twin booms support the tail section and produce an estimated drag coefficient of

$$\left(C_{D_o}\right)_b = .0006 \qquad (16)$$

The total airplane drag coefficient is now estimated by a drag-buildup method as

$$C_D = \left(C_{D_o}\right)_w + \left(C_{D_o}\right)_t + \left(C_{D_o}\right)_p + \left(C_{D_o}\right)_b + \frac{C_L^2}{\pi AR e} \qquad (17)$$

where the final term accounts for lift-dependent drag. The airplane efficiency factor e is estimated from a compilation of over 300 current sailplane configurations,[16] and for the present analysis is given by

$$\begin{aligned} e &= .9 \quad (AR \leq 20) \\ e &= 1.2 - .015\ AR \quad (AR > 20) \end{aligned} \qquad (18)$$

For given aspect ratio, equation (17) is used to calculate drag coefficient and endurance parameter as a function of lift coefficient. Referring to Fig. 5, the algorithm then calculates a required endurance parameter $C_L^{1.5}/C_D$, based on the assumed wing loading and the thrust power available per unit wing area

$$\frac{C_L^{1.5}}{C_D} = \sqrt{\frac{2}{\rho}\left(\frac{W_{tot}}{S_w}\right)^3 \frac{1}{P_{prop}}} \qquad (19)$$

where $P_{prop} = 5.5\ (S_w) - 800$ (See Fig. 4).

Next, the maximum endurance parameter based on the estimated vehicle aerodynamics is compared to that value. If no match exists, the airplane wing area (and aspect ratio, by equation (13)) is increased and a new endurance parameter function is

evaluated. The smallest wing area that produces an endurance parameter match is a solution. If no match is found after varying area, a higher wing loading is selected and the process repeated until a match is obtained. In the present analysis, program calculations are terminated if wing area exceeds 3500 ft^2 or aspect ratio exceeds 40.

Cruise flight is possible only at the lift coefficient corresponding to the matched endurance parameters. Further wing area (and aspect ratio) increase can produce endurance parameters which exceed the required value. This allows for a range of usable lift coefficients, thereby expanding the altitude-velocity envelope of the airplane.

The lift coefficients in this analysis are limited by a requirement to hold station against 95 percentile winds; therefore

$$C_{L_{max}} \leq C_{L_{wind}} = \frac{W_{tot}}{S_w}\left(\frac{2}{\rho V^2_{wind}}\right) \qquad (20)$$

Only calculated endurance parameters which do not exceed $C_{L_{max}}$ are valid in the analysis. Reference 17 presents seasonal high-altitude wind data in percentile form; i.e., percentage of time the wind speed is less than or equal to a chosen value. For the Tucson, Arizona study area, 95 percentile summer winds are as shown in Fig. 6. $C_{L_{max}}$ can be increased by flying higher (in the altitude range given) or by increasing the total wing loading.

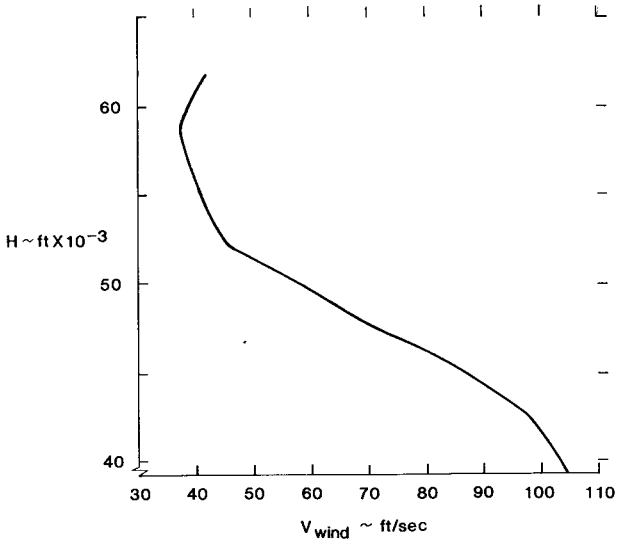

Fig. 6 Summertime 95-percentile wind profile in vicinity of Tuscon, Arizona (Ref. 17).

Parametric Sizing Results

Parametric airplane sizing results are now introduced for the reference mission based on the nominal altitude of 49,200 ft (15 km). Figure 7 presents aspect ratio vs. wing area solutions to equation (3) based on constant airframe wing loading W_{af}/S_w. Note that the "airframe" curves, by definition, are independent of mission constraints or other subsystem characteristics. Superimposed on these curves are two additional sets of curves based on, respectively, total wing loading W_{tot}/S_w and number of night cycles flown N. These curves are the loci of minimum wing area "aerodynamic" solutions (see Fig. 5) which satisfy mission requirements (viz., cruise at nominal altitude at velocity $\geq V_{wind}$ on July 21 and satisfy all demands for power over a given number of night cycles). Only those sizing solutions above and to the right of the dashed lines are possible aerodynamically. Such solutions produce a range of useful lift coefficients for which the related endurance parameter equals or exceeds the value dictated by the cruise power condition. Because available solar power has been fixed by mission specification (date and latitude) and certain subsystem parameters (solar cell characteristics and array size) there is a one-to-one correspondence between wing area and system power output as indicated on Fig. 7. For continuous duty, fuel-cell power output is limited to 12 kw. As the figure shows, this power level enables up to five night cycles at 49,200 ft (15 km)

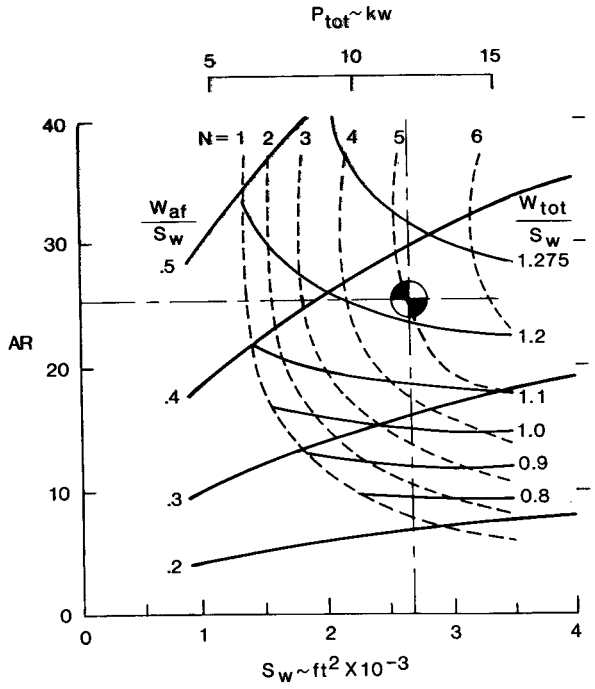

Fig. 7 Airplane sizing and aerodynamic solutions. Point design for reference mission shown by ◔ .

altitude. From these data, an airplane satisfying the reference mission requirements can be described in terms of aspect ratio, wing area, wing loading, and airframe weight loading. A full description of the airplane including performance characteristics, geometry, subsystem weights, and aerodynamic characteristics is presented in Table 1.

Before presenting a more extensive range of parametric data, some boundary conditions will be set. First, an upper limit of 25 on aspect ratio is deemed appropriate in light of present-day sailplane technology.[16] A maximum allowable wing area of 3500 ft^2 will provide for potential growth in power system output to about 15 kw. Finally, an altitude range of 39,400 ft (12 km) to 65600 ft (20 km) will accommodate variability in mission requirements.

Calculated data reflecting these limitations are presented in Fig. 8 for several values of N (number of night cycles) and AR (aspect ratio). For all values of AR and N, a minimum wing area exists near 47,500 ft. (14.5 km) altitude. Below this inflection, each N curve indicates that performance is wind-limited ($C_{L_{max}} > C_{L_{wind}}$); above the inflection, cruise velocity exceeds V_{wind}. Wing loading W_{tot}/S_w, not unexpectedly, is maximum at the inflection. In the absence of winds, performance is indicated by the dashed line extensions of each N curve. In these cases wing loading increases monotonically with decreasing wing area and cruise altitude.

Based on information presented on Fig. 8, for a given airplane (defined by aspect ratio, wing area, and wing loading) and number of night cycles, a range of operational altitudes is defined. For example, with AR=25, S_w=2220 ft^2, P_{tot}=10 kw, and N=1 (W_{tot}/S_w =.93) the operational ceiling is 63,300 ft (19.3 km) and a floor, dictated by prevailing winds, is 44,000 ft (13.4 km). These relationships can be more clearly seen on Fig. 9, where altitude envelopes are presented for values of N, AR, rated power P_{tot}, and wing loading W_{tot}/S_w.

The computer-aided algorithms described in Fig. 5 do not, in fact, account directly for continuous dumping of water during night flight. This deficiency in the endurance parameter matching algorithm introduces conservatism in terms of somewhat larger and heavier aircraft, reflecting the weight and power penalties incurred by carrying reactant product (water) until reactant depletion. However, intuition (and Breguet's endurance formula) suggests that potential increases in endurance due to water dumping are not significant until reactant weight becomes a large fraction of the total airplane weight. To illustrate, reactant mass fraction is shown on Fig. 10 as a function of altitude H, aspect ratio AR, number of night cycles N, and power level P_{tot} (hence, wing area). Note the growth in reactant mass fraction with H, N, and P_{tot}. Separate calculations for H=49,200 ft (15 km) produced the results presented in Fig. 11, where incremental growth in endurance $\Delta(NT)/NT$ is shown as a function of night cycles N. Note that a gain of one full night cycle does not occur until N reaches 6 and the power requirement reaches approximately 15 kw. The potential benefit from water dumping can be expected to increase at higher altitudes as reactant mass fraction increases (see Fig. 10).

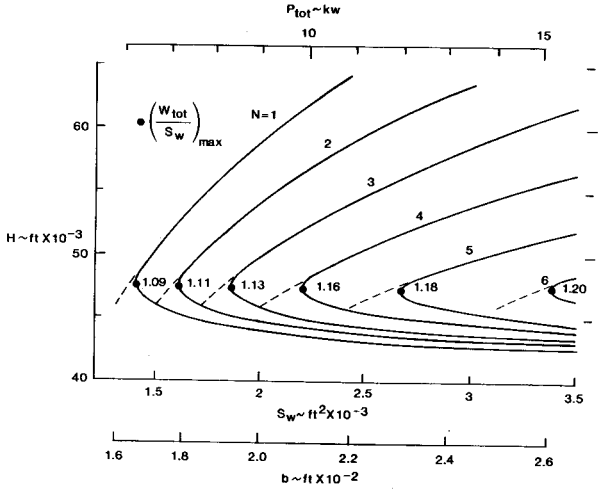

a) AR = 20

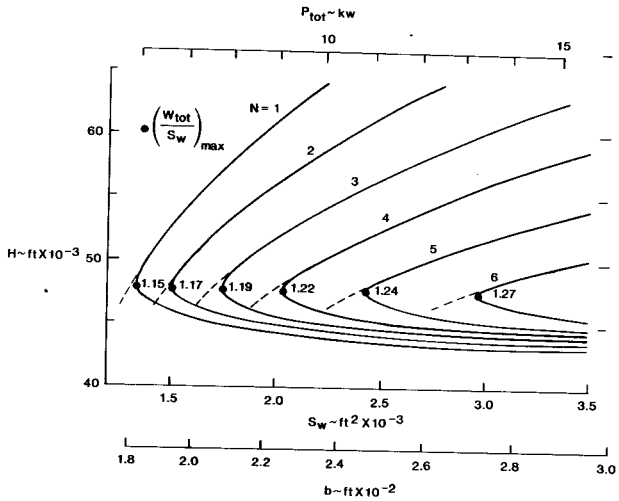

b) AR = 25

Fig. 8 Cruise endurance and altitude vs. airplane size and system power level for aspect ratios of 20 and 25.

Table 1. Airplane Characteristics for Reference Mission

Performance	
Cruise altitude, ft (km)	49,200 (15)
Maximum number of night cycles	5
Velocity, ft/sec	73.5
Thrust power available, w	6900
Power for avionics & payload, w	800
Solar array/fuel cell output, w	12,000
Propulsion drive efficiency	.75

Cruise Aerodynamics	
C_L	1.19
C_D	0.031
L/D	38.3
$C_L^{1.5}/C_D$	41.7
Chord Reynolds number:	
Root	1.16×10^6
Tip	0.58×10^6

Geometry	
Aspect ratio	24.95
Wing loading, lb/ft^2	1.216
Wing span, ft	257.5
Wing area, ft^2	2659

Weight

System	Pounds	Fraction
Airframe	989	.306
Propulsion drive	137	.042
Solar cells	399	.123
Fuel cell	300	.093
Reactants	626	.194
Tanks	494	.153
Radiator	48	.015
Avionics	140	.043
Payload	100	.031
TOTAL	3233	1.000

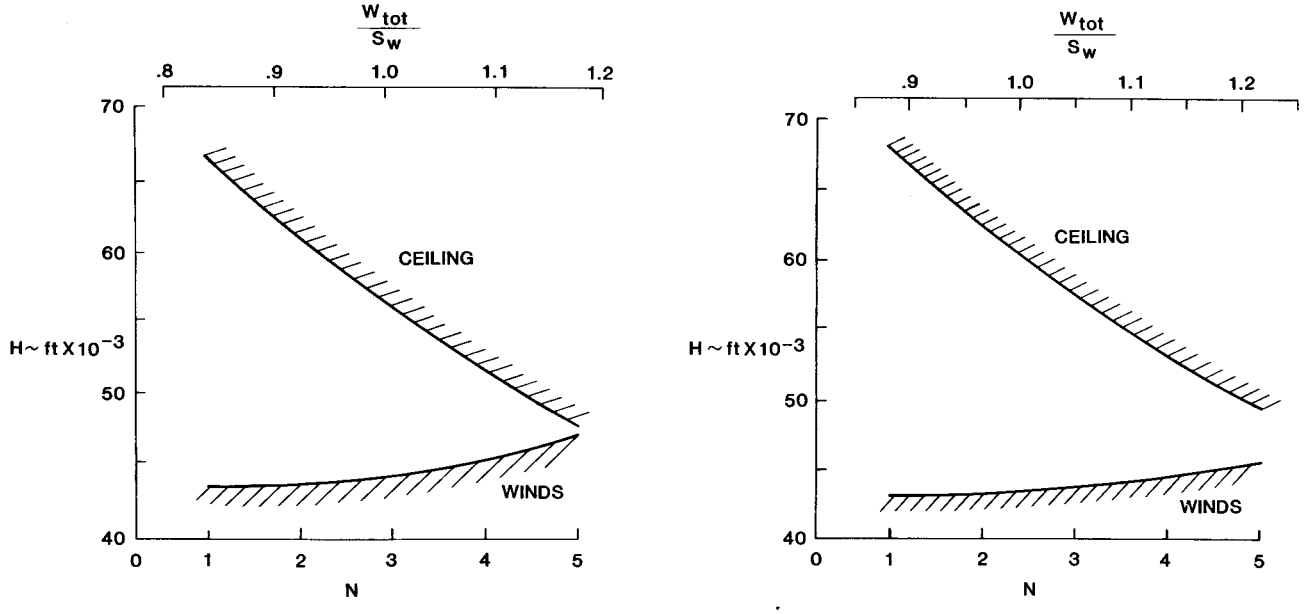

a) AR = 20

b) AR = 25

Fig. 9 Cruise altitude vs. endurance and wing loading for 12 kw power system and aspect ratios of 20 and 25.

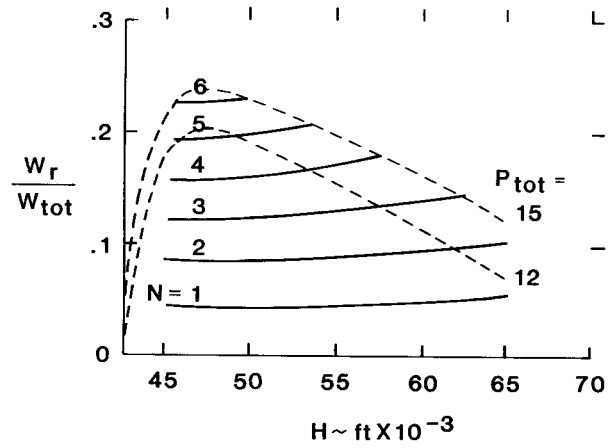

Fig. 10 Reactant mass fraction vs. cruise altitude, endurance, and power level for aspect ratio of 25.

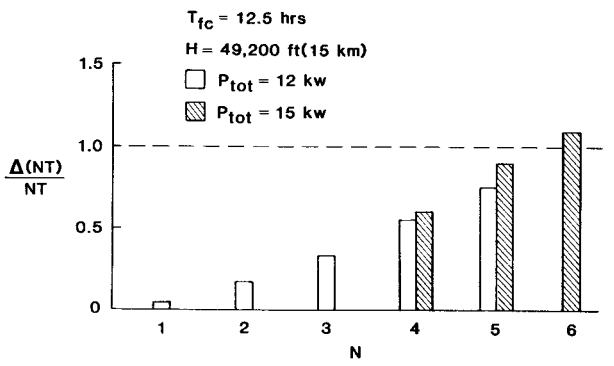

Fig. 11 Effect of in-flight water dumping on cruise endurence.

Concluding Remarks

A computational algorithm has been presented for estimating design parameters for a class of electric airplanes powered by direct solar energy by day and, by night, stored energy from a non-regenerative H_2-O_2 fuel cell of the type installed in the Space Transportation System Orbiter vehicle. The algorithm has been used to estimate airplane characteristics for a range of cruise altitudes, endurance values, and power levels. In addition, a particular airplane is sized for a summertime mission requiring endurance of several days at 49,200 ft (15 km) over south central Arizona.

Present results indicate that airplanes of this class tend to have very low wing loadings (0.9-1.3 lb/ft^2), and are relatively large (wing span > 200 feet), even with modest payload mass fractions. The effect of prevailing winds in the region and season of interest introduces a minimum cruise altitude below which the derived airplane cruise velocity becomes less than wind velocity, and station-keeping capability is lost. Because all onboard systems operate nominally at constant power levels, a substantial amount of solar energy is available around midday for aircraft maneuvering and payload augmentation.

The effect on endurance of dumping reactant waste product (water) overboard during night flight is found to be slight unless the airplane is designed to cruise for at least six night cycles, in which case reactant weight is a large fraction of total airplane weight.

Acknowledgement

Gratefully acknowledged is the contribution of John T. Suttles, Aero-Space Technologist of the Langley Research Center, who calculated the intra-atmosphere solar radiant flux densities used herein to compute solar cell power output.

References

1. MacCready, P. B., Lissaman, P. B. S.,Morgan, W. R., and Burke, J. D.: "Sun-Powered Aircraft Design," AIAA Paper 81-0916, May 1981.

2. Youngblood, J. W. and Talay, T. A.: "Solar-Powered Airplane Design for Long-Endurance, High Altitude Flight," AIAA Paper 82-0811.

3. Youngblood, J. W., Darrell, W. L., Johnson, R. W., and Harriss, R. C.: "Airborne Spacecraft - A Remotely Powered, High Altitude RPV for Environmental Applications," Electronic and Aerospace Systems Conference, Arlington, VA, October 9-11, 1979.

4. Tada, H. Y. and Carter, J. R., Jr.: "Solar Cell Radiation Handbook," Jet Propulsion Laboratory Publication 77-56, November 1, 1976.

5. Curran, P.: "A Samarium-Cobalt Motor-Controller for Mini-RPV Propulsion,"17th IECEC, 1982.

6. Stender, W.: "Sailplane Weight Estimation," OSTIV, 1969.

7. Hall, D. W., Hall, S. A., and Klingberg, R. D.: "Structural Sizing of a Solar Powered Aircraft," NASA Contractor Report 172313, 1984.

8. Stansell, J.: "Planes that Fly by the Sun," New Scientist, June 25, 1981.

9. Boucher, R. J.: "Project Sunrise," AIAA Paper 79-1264, June 1979.

10. Kuhn, Ira F., Jr., Reiss, K. W., Schubert, F. H., and Stedman, J. K.: "Regenerative Fuel Cell System Optimization," B-K Dynamics, Inc., Rockville, Maryland, Contract No. F33657-80-0343, June 15, 1981.

11. Hall, D. W., Fortenbach, C. D., Dimiceli, E. V., and Parks, R. W.: "A Preliminary Study of Solar Powered Aircraft and Associated Power Trains," NASA Contractor Report 3699, December 1983.

12. McMasters, J. H. and Palmer, G. M.: "At the Threshold of Man-Powered Flight," Astronautics and Aeronautics, September 1977.

13. Althaus, D.: "Stuttgarter Profilkatalog I," Der Universitatt Stuttgart, W. Germany, c. 1972.

14. Marsden, D. J.: "Sailplane Performance Estimation," Technical Soaring,Vol. 5, No. 3, March 1971.

15. Hoerner, S. F.: "Fluid Dynamics Drag,"Published by the author, c. 1965.

16. Soaring, Vol. 47, No. 11, November 1983.

17. Strganac, T. W.: "Wind Study for High Altitude Platform Design," NASA RP-1044, December 1979.